Structure and properties of amorphous silicon-metal alloys: II. The $Si_{1-x}Ti_x$ system

To cite this article: S J Gurman *et al* 2000 *J. Phys.: Condens. Matter* **12** 5981

View the article online for updates and enhancements.

Structure and properties of amorphous silicon–metal alloys: II. The $Si_{1-x}Ti_x$ system

S J Gurman†, B T Williams† and J C Amiss‡

† Department of Physics and Astronomy, University of Leicester, Leicester LE1 7RH, UK
‡ BMS, Sheffield Hallam University, Sheffield S1 1WB, UK

Abstract.   Structural and optical measurements have been made on a series of amorphous thin films of $Si_{1-x}Ti_x$ with $0 < x < 0.6$, prepared by RF sputtering. We present the results of structural studies using extended x-ray absorption fine structure (EXAFS) and small-angle x-ray scattering (SAXS), together with optical measurements of the band gap.

The EXAFS analysis gave interatomic distances, partial coordination numbers and Debye–Waller factors for the nearest neighbours of the two atom types. The Ti environment is found to be independent of composition for $x < 0.4$, with only the coordination numbers varying with composition at higher Ti contents. A small variation in the Si–Si interatomic distance was also found for $x < 0.4$.

Our samples show a metal–insulator transition (MIT) at about 6 at.% Ti. The SAXS results show that some phase segregation, on the 30 Å scale, occurs for low-Ti samples. We therefore suggest that the MIT should be interpreted in terms of a percolation theory involving regions of conducting amorphous Si_2Ti. We interpret the structural data in terms of such a phase segregated model, finding good agreement with the results of fits to experiment.

1. Introduction

The transition from semiconducting to metallic behaviour of certain alloys has been the subject of much interest from both a fundamental and technological point of view. Of special interest is the heavy doping of Si with transition metals because of the application to the microelectronics industry. The degree of control over conductivity in such materials has led to their application as components in integrated circuits [1]: by varying the metal content of these alloys it is possible to fabricate either metals or insulators.

The transition from semiconducting to metallic behaviour, the metal–insulator transition (MIT), is itself of fundamental interest. In silicon–metal amorphous alloys it occurs across a narrow threshold, usually at a metal content of around 15 at.% [2]. The mechanism of the MIT was originally thought to be electronic in origin, the alloying producing impurity levels deep within the intrinsic band gap inducing an Anderson type transition [3]. Recent structural reports, however, suggest that metallic behaviour occurs when regions of conducting material embedded in a non-conducting phase become large enough to percolate through the entire structure [4]. Without a more detailed knowledge of the short- and medium-range order, the MIT cannot be fully understood, yet few structural studies have been undertaken on these materials, and to our knowledge there have been no investigations into the structure of a-$Si_{1-x}Ti_x$.

We present here a structural investigation of amorphous $Si_{1-x}Ti_x$ alloys prepared in thin-film form across most of the composition range. We use the extended x-ray absorption fine

structure (EXAFS) to determine the local structure of our samples. Medium-range information, in particular studies of phase segregation, comes from small-angle x-ray scattering (SAXS). We combine our structural study with an optical study, on samples prepared at the same time as those used for the structural work, in order to try to correlate structural and electronic properties.

2. Sample preparation

Thin films of amorphous $Si_{1-x}Ti_x$, approximately 1 μm thick, were prepared by RF sputtering using a Nordiko NM-2000-T8-SE1 system. The pressure during sputtering was about 5 mTorr and the power applied to the target 200 W at a frequency of 13.56 MHz. The target consisted of a 10 cm disc of silicon with a number of squares of titanium foil placed on it. The number of these pieces was varied in order to vary the composition of the sputtered alloy. A variety of substrates was included in each deposition run: Mylar and copper foil for the EXAFS samples, aluminium foil for the SAXS samples and Corning 7059 glass for the optical samples.

The sample composition was determined using energy-dispersive x-ray analysis in a DS 130 scanning electron microscope. This method determines x to about ± 0.02, judging by the scatter of values obtained from different parts of the sample. All samples were found to contain about 2% argon, from the sputtering gas. The amorphicity of the samples was checked by transmission electron microscopy using a JEOL 100 CX instrument.

3. Experimental details and data analysis

EXAFS and SAXS measurements on the samples were performed at the synchrotron radiation source at the CLRC Daresbury Laboratory. The synchrotron was running at an electron energy of 2 GeV and beam currents of 150–250 mA during all experiments.

3.1. EXAFS measurements

The Si K edge was measured on station 3.4. This station has a chromium plated pre-mirror which provides a high energy x-ray cut-off at about 4 keV to minimize harmonic contamination. The energy of the x-ray beam was defined using an InSb(111) double-crystal monochromator. Absorption at the sample was measured by the electron drain current method: for this technique to be used the samples must be deposited on a conducting (here copper) substrate. The Ti K-edge data were taken on station 7.1 using the standard transmission geometry. This station has a silicon(111) double-crystal monochromator. Harmonic rejection was achieved by a 50% detuning off the Bragg peak. Sample absorption was measured using two ion chambers filled with an Ar/He gas mixture of compositions set to give 20% absorption for the I_0 monitor and 80% absorption for the I_t monitor. The absorption step at the Ti K edge was set close to unity by folding the samples to give the appropriate amount of titanium in the beam. For this reason these samples were deposited on thin Mylar substrates.

3.2. SAXS measurements

SAXS measurements were made on station 8.2. This provides a highly collimated x-ray beam of wavelength 1.5 Å from a Ge(111) monochromator. The detector was a 512-wire proportional counter, the quadrant detector, with a maximum count rate of 10^5 photons s^{-1}. A camera length of 1.5 m was used so that the maximum scattering vector measured was 0.5 Å^{-1}. The first 0.02 Å^{-1} of this range is obscured by a beam stop, to prevent the direct beam from overloading

the detector. The scattering vector was calibrated using a standard collagen sample. Each SAXS spectrum results from a 2 min collecting time. Aluminium substrates were used for the SAXS samples, since these give a smooth background in the SAXS region.

3.3. Optical measurements

Optical measurements at visible and near infra-red photon energies were made using a double-beam Perkin–Elmer 330 instrument. The absorption coefficient α and refractive index $n(E)$ were determined by standard transmission and reflection methods.

3.4. Data analysis

The EXAFS data were calibrated, background subtracted and analysed using standard Daresbury packages EXCALIB, EXBACK and EXCURV92 respectively. EXCALIB converts monochromator positions to x-ray energy and the detector signals to an absorption coefficient. EXBACK fits the pre- and post-edge regions by low-order polynomials in the standard manner to extract the oscillatory EXAFS function.

The package EXCURV92 uses a least-squares curve-fitting procedure to compare theoretical and experimental spectra, with the structural parameters (distance, co-ordination number, Debye–Waller factor and atom type) of the near neighbours as fitting parameters. The theoretical spectra were calculated using fast curved wave theory [5], including single scattering only. The Hedin–Lundqvist exchange potential and von Barth ground state potential were used to calculate the scattering phase-shifts for both edges. A standard Ti foil was used to determine the amplitude reduction factor (AFAC) to be used during analysis of Ti K-edge data: this was found to be 0.9. AFAC for the Si K edge was found to be 0.95 using the a-Si sample, where a coordination of four is expected, as a standard. The Hedin–Lundqvist potential is known to give a good description of inelastic processes in the EXAFS energy range, so AFAC should be very close to unity. The program also determines the uncertainties in the fitted parameters and also determines whether a shell of atoms *significantly* improves the fit, using the Joyner method [6]. The uncertainties quoted here are always $\pm 2\sigma$ (95% confidence). All shells described improved the fit index significantly.

SAXS data reduction used the Daresbury XOTOKO package, which normalizes, calibrates and background subtracts the data. Most of the background comes from the substrate with some contribution from windows and air scatter: background subtraction used data from a blank aluminium substrate to deal with all of these. The data were analysed in terms of Guinier theory for the low-q structure (due to isolated structures) and a simple correlation length method for the high-q structure, which we believe to be due to phase segregation.

The optical analysis was based entirely on the measured absorption coefficient α. Two methods were used to determine the band gap: choice of a standard absorption and a Tauc analysis. The standard absorption used to define the band gap was $\alpha = 10^4$ cm^{-1}. The Tauc analysis assumes parabolic forms for the band edges and so derives the expression

$$E\alpha(E) = C(E - E_T)^2$$

for the energy variation of the absorption coefficient close to the absorption edge. The Tauc energy E_T, obtained from a plot of $(E\alpha)^{1/2}$ against E is then a measure of the band gap. The two analyses give very similar results for the optical band gap.

4. Results

4.1. EXAFS results

An example of Ti K-edge EXAFS data is shown in figure 1. For each data set, a two-shell fit with Si in the first shell and Ti in the second was found to be appropriate. Good quality data extending from 1 to 12 $Å^{-1}$ for most spectra meant a fit index of around 10–20 could be obtained.
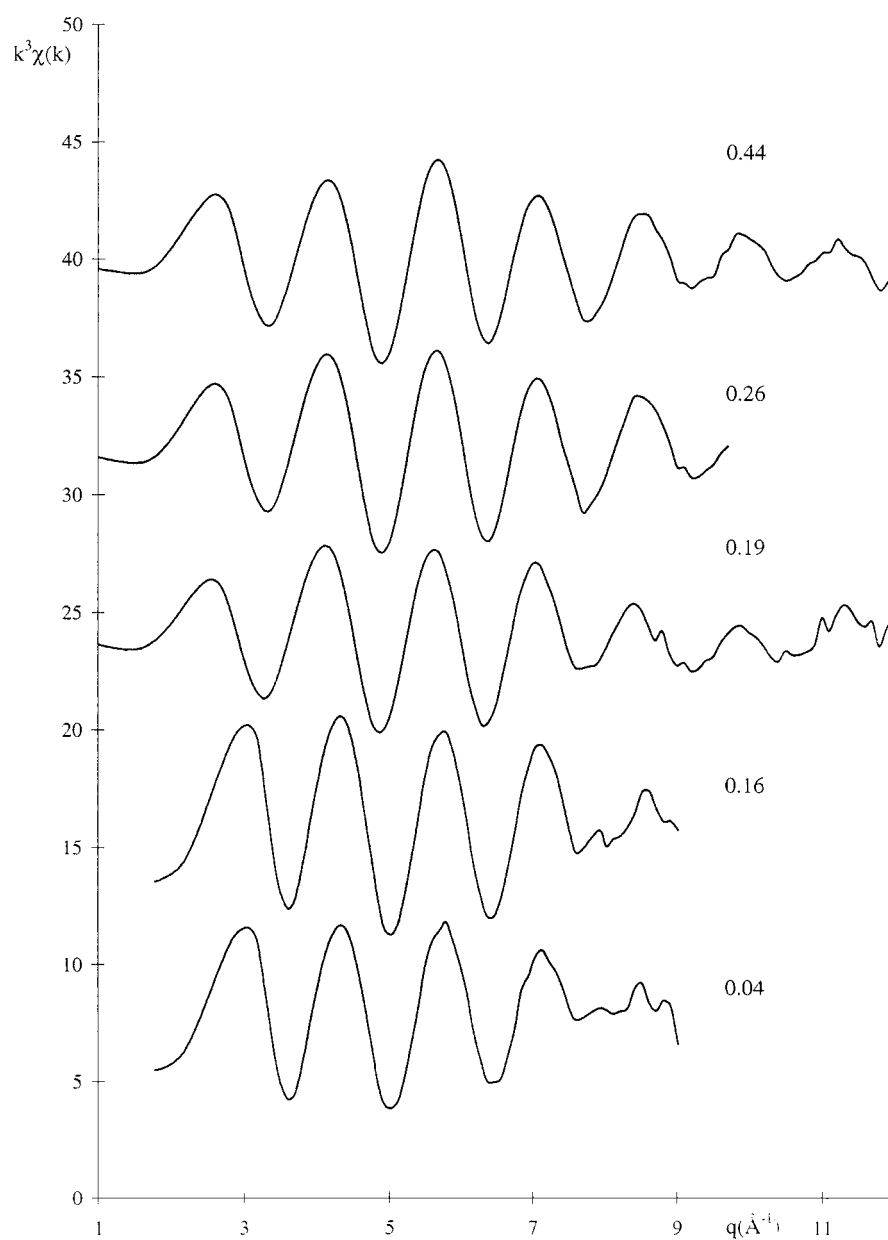

Figure 1. Ti K-edge EXAFS spectra.

The Si K-edge data, not shown, were of a considerably lower quality than Ti K-edge data, due in part to the drain-current method used. Analysis was hampered by a short data range of $1–9$ Å^{-1}, hence fit indices of 30–50 were typical. Despite the shortcomings of the data, a two-shell fit was found to be appropriate, i.e. fitting a second shell reduced the fit index by 10% or more, with the exception of the $x = 0.26$ sample where only a single Si shell could be fitted. Table 1 summarizes the EXAFS results obtained for $Si_{1-x}Ti_x$.

Table 1. EXAFS results for amorphous $Si_{1-x}Ti_x$ thin films. The uncertainties quoted are $\pm 2\sigma$ (95% confidence).

x	R (Å) (SiSi)	R (Å) (SiTi)	R (Å) (TiSi)	R (Å) (TiTi)	N (SiSi)	N (SiTi)	N (TiSi)	N (TiTi)	σ^2 (Å^2) (SiSi)	σ^2 (Å^2) (SiTi)	σ^2 (Å^2) (TiSi)	σ^2 (Å^2) (TiTi)
0.00	2.34	—	—	—	4.0	—	—	—	60	—	—	—
0.04	2.33	2.62	2.65	2.82	2.9	0.3	9.1	1.7	50	200	20	150
0.16	2.36	2.59	2.65	2.78	2.9	1.9	9.5	2.6	60	300	250	180
0.19	2.36	2.60	2.66	2.80	2.2	2.5	9.3	2.2	40	400	240	140
0.26	2.37	—	2.66	2.79	2.1	—	9.5	1.9	30	—	230	120
0.44	2.37	2.60	2.66	2.80	0.8	5.1	8.0	1.5	20	200	200	130
0.51	2.38	2.58	2.66	2.80	1.3	4.8	8.0	1.9	30	200	250	140
0.54	2.37	2.61	2.66	2.82	1.2	5.0	5.6	2.2	50	250	200	140
									$\times 10^{-4}$	$\times 10^{-4}$	$\times 10^{-4}$	$\times 10^{-4}$
	± 0.02	± 0.02	± 0.02	± 0.02	± 0.5	± 1.0	± 0.5	± 0.5	± 20	± 50	± 30	± 30

Atoms of Si in the crystal are 2.34 Å apart: the value for amorphous Si is 2.35 Å [7]. From table 1 we see that the Si–Si bond in a-$Si_{1-x}Ti_x$ remains at approximately this length to within experimental error, with some evidence of a small, slow rise with increasing Ti content. The Ti–Ti bond length was found to be shorter than the value of 2.91 Å in metallic Ti [7] at 2.80 ± 0.02 Å, invariant across the composition range.

The Si–Ti bond length also remained constant in all samples but was found to be slightly higher when viewed from Ti atoms (2.66 ± 0.02 Å) than when measured with respect to Si (2.60 ± 0.02 Å), probably due to a slight mismatch in the calculation of phase shifts at each edge. We suggest the value 2.64 ± 0.03 Å, being slightly weighted towards the better Ti results. This value compares well with the sum of the covalent radii, 2.63 Å [7], indicating covalently bonded Si and Ti.

The Si–Ti and Ti–Si partial coordinations for $x \geqslant 0.44$ are not quite consistent with one another, probably due to the poorer Si K-edge data. These coordination numbers must be related by the consistency condition $(1 - x)N_{SiTi} = xN_{TiSi}$ derived from the equality of the number of Si–Ti bonds when viewed from either end. In the discussion, we prefer the values derived from the Ti data.

Figure 2(a) shows the Si–Si distance and figure 2(b) shows the partial Si–Si and Si–Ti coordination numbers respectively, as functions of composition. In pure silicon, Si is surrounded by four other Si atoms. As Ti is added, the number of Si atoms falls, these being replaced by Ti atoms, with a steady increase in the total Si coordination. At very high Ti content, Si probably becomes almost close packed. This idea is supported by work done on the bulk a-$Si_{1-x}Ti_x$ glass [8] where at $x = 0.84$, Si is surrounded by 9.4 Ti atoms. From the results given in table 1 it can be seen that Ti is close packed, its environment independent of composition, surrounded by about nine Si atoms and two Ti atoms for $x \leqslant 0.3$. At higher Ti contents, the Ti–Si coordination falls steadily, the total Ti coordination being constant at about eight to 10. This apparently high number of Si atoms for $x \leqslant 0.6$ is in agreement with data from the crystal $TiSi_2$ where $N_{TiSi} = 10$ and TiSi where $N_{TiSi} = 6$ [9].
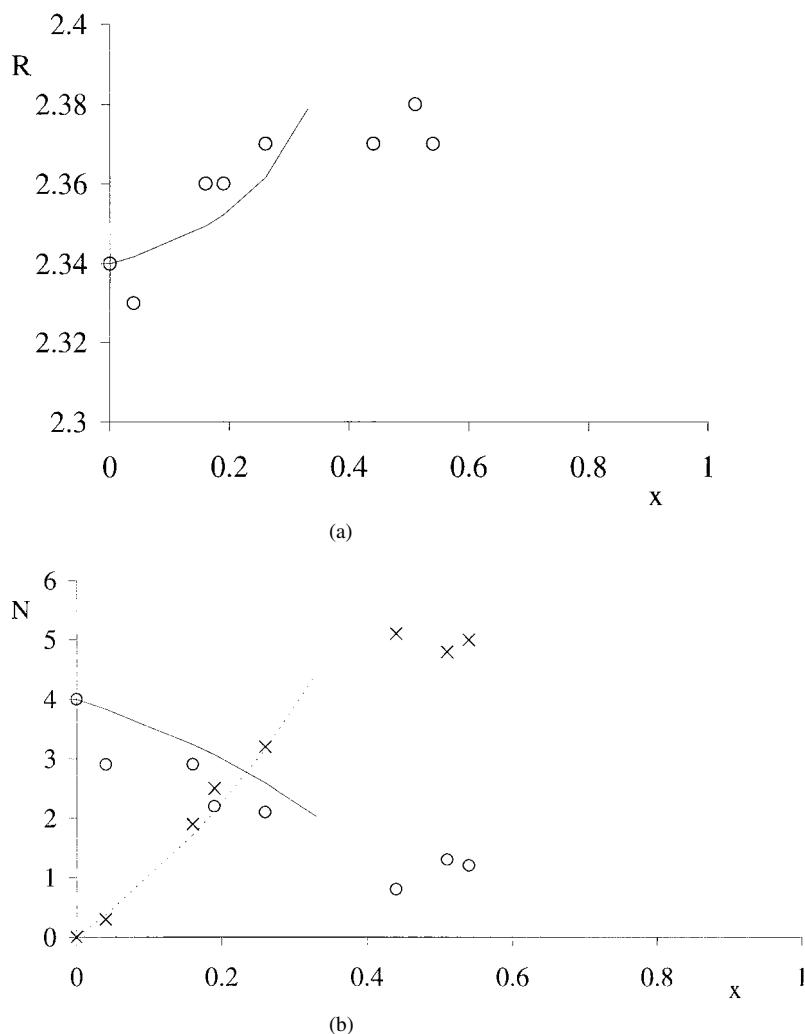
Figure 2. (a) Si–Si distance determined experimentally (O). The line is the prediction of the model discussed in the text. (b) Partial Si–Si (O) and Si–Ti (×) coordination numbers as determined by fitting to the EXAFS data. The lines are the predictions of the model discussed in the text. Solid line Si–Si; dashed line Si–Ti.

The Debye–Waller factors (the mean square variation in interatomic distance) σ^2 for our samples are also shown in table 1. Values obtained from the Si absorption edge are clearly less reliable than their Ti edge counterparts, which is to be expected considering the relative quality of each raw data spectrum. The Debye–Waller factors are found to be independent of composition with values of $\sigma^2_{SiSi} = (45 \pm 20) \times 10^{-4}$ Å^2 and $\sigma^2_{TiTi} = (140 \pm 30) \times 10^{-4}$ Å^2.

The room-temperature thermal contribution to σ^2_{SiSi} is known to be 40×10^{-4} Å^2 [10] indicating that there is almost no static disorder in this bond for our samples: this is well known in pure amorphous silicon. It must be noted however that the total electron yield measurements only probe the top 50–100 Å of the sample and therefore the effect may be confined to the surface. Using the Debye model of atomic vibrations with a Debye temperature of 428 K for Ti to calculate the thermal contribution to the Ti–Ti bond, we find that $\sigma^2 = 40 \times 10^{-4}$ Å^2.
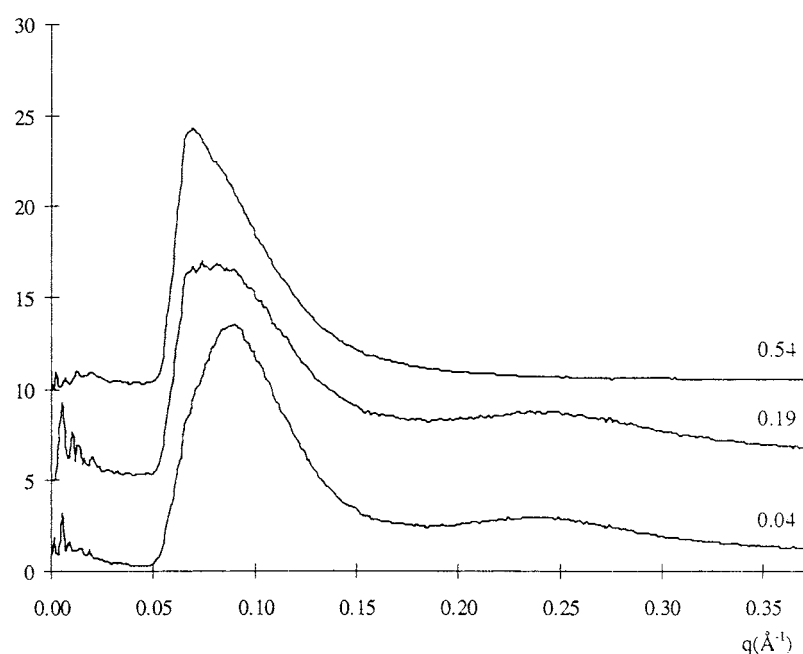
Figure 3. SAXS data for three $Si_{1-x}Ti_x$ samples. The cut-off below $k = 0.08$ Å^{-1} is due to the beam-stop.

When compared with the experimental value of 140×10^{-4} Å^2, it can be inferred that most of the variation arises from static disorder rather than thermal effects. The degree of static disorder corresponds to an RMS variation in the Ti–Ti distance of about 0.1 Å.

Values of σ^2 for Ti–Si are constant across the composition range at about 250×10^{-4} Å^2 and the values obtained from the two edges are consistent, albeit with large errors. Under the assumption that the Ti–Si bond will behave thermally in a similar manner to the homopolar bond, we expect the deviation in the Ti–Si bond length associated with thermal vibrations to be approximately $(40$–$50) \times 10^{-4}$ Å^2, indicating that the large observed Debye–Waller factor is largely due to static disorder. For this bond the RMS variation in distance due to static disorder is about 0.15 Å. Thus we see that both the Ti–Ti and the Ti–Si nearest neighbour peaks in the pair distribution function are rather broad.

4.2. SAXS results

Sample SAXS spectra, normalized and background subtracted, are shown in figure 3. The main feature of each spectrum is the large peak at 0.08 Å^{-1}, with a sharp cut-off at 0.05 Å^{-1} due to the beam-stop. The peaks are of approximately equal amplitude and shape, indicating that the inhomogeneities present occur in the same quantities and are of the same size, independent of Ti content. This provides evidence in favour of isolated voids as the origin of the observed scatter as they can be introduced during sample fabrication in the form of bubbles of Ar sputtering gas. Their characteristics will be a function of sputtering conditions rather than chemical composition [11]. A Guinier analysis [12] of this peak shows the dimension of the voids to be about 35 ± 2 Å.

The two samples containing 4 at.% and 19 at.% Ti display a weak second peak at 0.24 Å^{-1} while the sample containing 54 at.% Ti does not. This signals the presence of non-disperse

regions of differing electron density [13]. The compositional dependency of the amplitude of this peak suggests that we could be seeing the manifestation of phase separation. The SAXS data suggests that the segregation is probably into an amorphous Si_2Ti (or possibly SiTi) phase in an amorphous Si matrix. The position of the second peak indicates a correlation length [13] of about 25 Å for this segregation.

4.3. Optical studies

Measurement of the optical absorption properties of a sample indicates the extent of the band gap and hence whether the material is metallic or semiconducting. It was found that all samples where $x \geqslant 0.16$ were highly absorbing, indicating metallic behaviour. The absorption coefficient of the two samples with $x = 0.00$ and $x = 0.04$ fell rapidly at low photon energies, indicating semiconducting behaviour. A standard measure of the gap is taken as the energy where the absorption coefficient $\alpha(E) = 10^4$ cm^{-1}, denoted E_{04}. This was found to be 1.4 ± 0.2 eV for a-Si, a little higher than the crystalline value of 1.2 eV [11]. This is surprising because the band gap is expected to be smaller in amorphous materials due to the disorder induced effect of band tailing into the gap. This observation may reflect the fact that E_{04} is not a measure of the true gap, but of the energy separation of states higher in the valence and conduction bands. E_{04} for the sample where $x = 0.04$ was found to be 0.5 ± 0.2 eV.

A Tauc analysis showed a decrease in the width of the band gap, E_{Tauc}, from 1.3 ± 0.2 eV for a-Si to 0.3 ± 0.2 eV for a-$Si_{0.96}Ti_{0.04}$. The theory behind Tauc analysis assumes parabolic band edges, which may not be the case. For this reason we have adopted E_{04} as a measure of the band gap.

An attempt to show the composition dependence of the band gap is hampered by a distinct lack of data points. However, by assuming a linear relationship, it appears that the gap closes at $\sim 6 \pm 2$ at.% Ti. We take this value as the critical concentration at which the MIT occurs.

5. Discussion

Inspection of the Si and Ti partial coordinations suggests two distinct types of behaviour:

(i) in the composition range $0 \leqslant x \simeq 0.3$ the Ti environment is independent of composition. None of the structural parameters determined from the EXAFS fits to the Ti K edge varies significantly in this regime. In the same region, the Si–Si coordination number falls steadily whilst Si–Ti rises. The Si–Si distance also rises slowly and just significantly. Similar results have been noted by us [14] and by Edwards *et al* [15] in the Si–Ni:H system.

(ii) For Ti contents greater than about 30 at.%, the Ti–Si coordination steadily falls. The Si–Si coordination is low, whilst Si–Ti rises rapidly. Neither the distances nor the Debye–Waller factors change with composition in this region. Our results appear to match the diffraction data for $Si_{0.84}Ti_{0.16}$ [8].

The SAXS data indicate that phase segregation occurs for samples containing less than about 40% Ti. The phase segregation has a correlation length of about 25 Å.

We can combine all of these results in a simple model of the Si–Ti amorphous system. We suggest that at low Ti contents, our films are phase segregated, on the 30 Å scale, into a mixture of an amorphous Si_2Ti phase and an amorphous Si phase. Such a segregation occurs for all $x \leqslant 0.33$. Such a model gives an invariant Ti environment and a varying average Si environment for $x \leqslant 0.33$, as observed. In order to quantify the model, we assume that the amorphous Si phase has four Si–Si neighbours at 2.32 Å whilst the amorphous Si_2Ti phase

has two Ti–Ti neighbours at 2.80 Å, nine Ti–Si (and so 4.5 Si–Ti) neighbours at 2.64 Å and two Si–Si neighbours at 2.38 Å. This structure is consistent with our EXAFS results from the Ti K edge, and very similar to that found in crystalline Si_2Ti [16]. We can then predict the average structural parameters observed by EXAFS: these predictions are indicated by lines in figure 2. We see that the model, which is based on the structures of several group IV transition metal compounds, gives a good description of the coordination numbers observed. It also fits the interatomic distances, especially the slowly rising Si–Si distance, and the constant Si–Ti distance. In the model the Si–Si distance rises linearly from 2.34 Å at $x = 0.00$ to 2.38 Å at $x = 0.33$: such a trend is shown in the results given in table 1.

Further evidence for an a-Si, a-Si_2Ti mixture is provided by Gong *et al* [17] in their study of the Gibbs free energy (ΔG) of the Si–Ti system where they report that there are three distinct regions in the ΔG–x curve. The first for $0 \leqslant x \leqslant 0.23$, is where a mixture of crystalline Si and an amorphous alloy has a lower ΔG than a single-phase amorphous alloy (although our EXAFS data from the Si K edge show little structure beyond the first maximum in the RDF, indicating that there is no crystalline phase present in our films). For $0.23 \leqslant x \leqslant 0.83$, a single phase should be a more stable state. Indeed, our sample containing 54 at.% Ti shows no phase separation. For $0.83 \leqslant x \leqslant 1.0$, a mixture of crystalline Ti and an amorphous alloy has a lower ΔG and should therefore be more stable. The correlation is clearly not perfect, but is suggestive.

Guinier analysis of SAXS data also revealed the presence of widely separated inhomogeneities, of approximately 35 Å in size with characteristics invariant across the composition range. This leads us to attribute the scattering in the Guinier region to neutral inclusions of Ar atoms introduced during the sputtering process, as opposed to chemically dependent inhomogeneities such as phase segregation. Conclusive results can only be obtained by performing anomalous SAXS which scans the energy of the incident x-ray beam through an absorption edge, allowing the contribution of each element to the scattering pattern to be identified.

If the samples are phase segregated then a percolation model is appropriate for the MIT, assuming that one of the phases is metallic. We find a metal–insulator transition occurring at around 6 at.% Ti for a-$Si_{1-x}Ti_x$. This is much lower than the critical concentration (N_c) found in other similar systems, e.g. a-SiAu where $N_c = 14$ at.% Au [18], a-SiMn has an N_c of 17 at.% Mn [19] and a-SiFe is reported to undergo the MIT at 16 at.% Fe [20]. These alloys are believed to be single phase. The percolation threshold for the MIT occurs when about 16% of the sample by volume exists in the conducting phase [21]. If the conducting phase is indeed a-Si_2Ti, and if this is metallic and of the same density as the crystalline form (which is metallic and has a density of 4080 kg m^{-1} [16]), then the MIT should occur at about 16% by volume Si_2Ti content, or about 5% Ti content by atomic composition. This is in line with our determination and accounts for the low value of the metal content at the MIT.

The conjecture is that the MIT in our samples occurs when pockets of a conducting compound (Si_2Ti) interconnect at a percolation threshold. This argument is discussed in depth by Regan *et al* [4], who invoke a percolation argument rather than an Anderson transition model to explain the MIT transition in samples of a-$Ge_{1-x}Fe_x$.

6. Conclusion

We have set out to characterize the short- and medium-range structure of a-$Si_{1-x}Ti_x$ and in so doing perhaps arrive at a better understanding of the metal–insulator transition. EXAFS and SAXS methods were used to obtain structural information. Optical spectroscopy was used to determine the critical metal content at which the MIT occurs: this was found to be at about 6 at.% Ti.

Our results indicate that Si co-exists as a tetrahedral random network and as an a-Si$_2$Ti alloy, the former in diminishing quantities as Ti is added. This idea is supported by results from our SAXS experiments where evidence indicating the presence of two phases at low Ti content was found. If this is the case then a percolation theory of interconnecting conducting regions of a-Si$_2$Ti would have to be considered as a model of the MIT.

Acknowledgments

References

[1] Reader A H, van Ommen A H, Weijs P J W, Wolters R A M and Oostra D J 1993 *Rep. Prog. Phys.* **56** 1397
[2] Colver M M 1977 *Solid State Commun.* **23** 333
[3] Mott N 1974 *Metal–Insulator Transitions* (London: Taylor and Francis)
[4] Regan M J, Rice M, Fernandez van Raap M B and Bienenstock A 1994 *Phys. Rev. Lett.* **73** 1118
[5] Gurman S J, Binsted N and Ross I 1984 *J. Phys. C: Solid State Phys.* **17** 143
[6] Joyner R W, Martin K J and Meehan P 1987 *J. Phys. C: Solid State Phys.* **20** 4005
[7] Kittel C 1971 *Introduction to Solid State Physics* 4th edn (London: Wiley) p 39
[8] Lamparter P, Habenschuss A and Narten A H 1986 *J. Non-Cryst. Solids* **86** 109
[9] Hansen M 1958 *Constitution of Binary Alloys* 2nd edn (London: McGraw Hill) p 1197
[10] Bayliss S C and Gurman S J 1991 *J. Non-Cryst. Solids* **127** 174
[11] Long D 1968 *Energy Bands in Semiconductors* (New York: Interscience)
[12] Guinier A and Fournet G 1955 *Small-Angle Scattering of X-Rays* (New York: Wiley)
[13] Cahn J W 1965 *J. Chem. Phys.* **42** 93
[14] Williams B T, Gurman S J, Baker S H and Davis E A 2000 *J. Phys.: Condens. Matter* at press
[15] Edwards A M, Fairbanks M C, Newport R J, Gurman S J and Davis E A 1989 *J. Non-Cryst. Solids* **113** 41–50
[16] Trotter J (ed) 1977 *Structure Reports for 1977 (Metals and Inorganic Sections vol 43A)* (Utrecht: Oosthoek, Scheltema and Holkema) p 96
[17] Gong S F, Robertson A, Hentzell H T G and Li X-H 1990 *J. Appl. Phys.* **68** 4535–41
[18] Kishimoto N and Morigaki K 1979 *J. Phys. Soc. Japan* **46** 846
[19] Shimizu T, Kumeda M, Watanabe I and Noumi Y 1960 *J. Non-Cryst. Solids* **35/36** 645
[20] Sano Y, Iwami M, Hiraki A and Morigaki K 1982 *Japan. J. Appl. Phys.* **21** L291
[21] Zallen R 1983 *Physics of Amorphous Solids* (New York: Wiley)